

NEUTRONLESS ^{10}Be -ACCOMPANIED TERNARY FISSION OF ^{252}Cf

A. Săndulescu^{1,2,3,4,5)}, F. Cârstoiu^{1,2,5)}, Ş. Mişicu^{1,2,5)}, A. Florescu^{1,3,4)},
A.V. Ramayya^{3,4)}, J.H. Hamilton^{3,4)}, J.K.Hwang^{3,4)}, and W. Greiner^{3,4,5)}

- 1) Institute of Atomic Physics, Bucharest, P.O.Box MG-6, Romania
- 2) Gessellschaft für Schwerionenforschung mbH, 64291 Darmstadt,
Wixhausen, Germany
- 3) Physics Department, Vanderbilt University, Nashville, TN 37235, USA
- 4) Joint Institute for Heavy Ion Research, Oak Ridge, TN 37831, USA
- 5) Institut für Theoretische Physik der J.W.Goethe Universität,
D-60054, Frankfurt am Main, Germany

Abstract : A new type of decay corresponding to the neutronless ^{10}Be -accompanied fragmentation of ^{252}Cf is studied. We employ a cluster model similar to the model used for the description of cluster radioactivity. No preformation factors were considered. The ternary relative isotopic yields were calculated as the ratio of the penetrability of a given ternary fragmentation over the sum of penetrabilities of all possible ternary neutronless fragmentations. The corresponding barriers between the light and heavy fragment and between the ^{10}Be cluster and the two heavier fragments were computed with the help of a double folding potential generated by M3Y- NN effective interaction and realistic fragment ground state deformations. Also, we studied the influence of the fragment excitation energies on the yields, by including the level densities and the β -stretching of the fragments. The new phenomenon could be experimentally observed by the triple gamma coincidence technique between the fragments and ^{10}Be .

PACS number : 25.85.Ca,27.90.+b

1. Introduction

The cold (neutronless) fission of many actinide nuclei into fragments with masses from ≈ 70 to ≈ 160 is nowadays a well studied phenomenon [1-8]. Since the final nuclei are generated in their ground states or some low excited states, these decays were soon related to the spontaneous emission of light nuclei (cluster radioactivity) such as alpha particles and heavier clusters ranging from ^{14}C to ^{34}Si [9,10]. All these experimental findings confirmed the theoretical predictions regarding the cold rearrangement processes of large groups of nucleons from the ground state of an initial nucleus to the ground states of two or three final fragments [11,12]. Indeed, some fragmentations of heavy nuclei involving more than two final fragments have been also observed. In the spontaneous and thermal neutron induced fission of heavy nuclei the third fragment is usually a light charged particle (LCP), the most probable being an alpha particle [13-16]. Heavier clusters like ^{10}Be , ^{14}C , ^{20}O , ^{24}Ne , ^{28}Mg and ^{34}Si [15] have also been detected in these hot fragmentations.

It is very important to establish theoretically and experimentally if cold (neutronless) ternary fragmentations similar to the cold binary ones are existing in nature. This new phenomenon will be equivalent to cluster radioactivity during the fission. Such cold ternary decays will produce all three fragments with very low or even zero internal excitation energy and consequently with very high kinetic energies. Their total kinetic energy $TKE = Q_t - TXE$ will be close to the corresponding ternary decay energy Q_t . In order to achieve such large TKE values, the three final fragments should have very compact shapes at the scission point and deformations close to those of their ground states, similar to the case of cold binary fragmentations [17,18].

The first direct observation of cold (neutronless) binary fragmentations in the spontaneous fission of ^{252}Cf was made [4,5], by using the multiple Ge-detector Compact Ball facility at Oak Ridge National Laboratory, and more recently with the Gammasphere consisting of 72 detectors [5,6].

From these Gammasphere data, it was possible to observe for the first time directly the cold (neutronless) alpha ternary fission yields. Only the correlations between the two heavier fragments were observed unambiguously, by using the triple-gamma coincidence technique. Also, in these cold fragmentations, some indications of third light fragments as ^6He , ^{10}Be and ^{14}C clusters were possible [19,20]. Soon direct correlations with the gamma rays emitted from LCP may be also possible. In this way the accidental coincidences of fission fragments with the binary partners, which represents the main background for ternary fragmentations, are eliminated.

In the present paper, based on a cluster model, we estimated the relative isotopic yields for the spontaneous cold (neutronless) ^{10}Be -ternary fission of ^{252}Cf . These isotopic yields are given by the ratio of the penetrability through the potential barrier between the two final heavier fragments for a given mass and charge splitting, over the sum of penetrabilities for all possible (neutronless) fragmenta-

tions. We studied the influence of the fragment excitation energies on the yields, by including the level densities and the β -stretching of the fragments. The corresponding barriers were evaluated using the double folding potential with M3Y nucleon-nucleon effective interactions and realistic ground state deformations including the octupole and hexadecupole ones [6, 21]. The light cluster was considered as spherical. We assumed first that the two heavier fragments penetrate the thin barrier existing between them and later-on the LCP is jumping over the potential barrier defined by the interaction between the light cluster and the two deformed heavier fragments. We expect that the fragment mass distribution in cold ^{10}Be ternary fission of ^{252}Cf to be similar with that from cold binary fission of ^{242}Pu .

2. Potential Barriers

In the present paper we consider a cluster model, similar to the one-body model used for the description of cluster radioactivity [9]. We assume that the initial nucleus is already separated into three parts, two heavier ones and a cluster, i.e. no preformation factors for the fragments are taken into account. An advantage of this model is that the barrier between the two heavier fragments and the barrier between the light cluster and the heavier fragments can be calculated quite accurately due to the fact that the touching configurations are situated inside of the barriers. The Q values and the deformation parameters contain all nuclear shell and pairing effects of the corresponding fragments.

We have calculated the barriers using the double folding model for heavy ion interaction

$$V_F(\mathbf{R}) = \int d\mathbf{r}_1 d\mathbf{r}_2 \rho_1(\mathbf{r}_1) \rho_2(\mathbf{r}_2) v(\mathbf{s}) \quad (1)$$

where $\rho_{1(2)}(\mathbf{r})$ are the ground state one-body densities of the fragments (not necessarily spherical) and v is the NN effective interaction. The separation distance between two interacting nucleons is denoted by $\mathbf{s} = \mathbf{r}_1 + \mathbf{R} - \mathbf{r}_2$, where R is the distance between the c.m. of the two fragments. For simplicity we have chosen the G -matrix M3Y effective interaction (see [22] for a review) which is representative for the so called local and density independent effective interactions. This interaction is particularly simple to use in folding models since it is parametrized as a sum of 3 Yukawa functions in each spin-isospin (S, T) channel. Only the isoscalar and isovector components have been retained in the present study for the central heavy ion interaction. The spin-dependent components have been neglected since for a lot of fragments involved in the calculation the ground state spins are unknown. Moreover, the spin-spin component of the heavy-ion potential is of the order $1/A_1 A_2$ and can be safely neglected here.

The M3Y interaction is dominated by the exchange component, therefore it is extremely important to include this component in the barrier calculation in an accurate way. The most important contribution comes from the one-nucleon knock-on exchange term, which leads to a nonlocal kernel. The range of the nonlocality

behaves as μ^{-1} , where $\mu = A_1 A_2 / (A_1 + A_2)$ is the reduced mass of the interacting system, and therefore the nonlocal potential is reduced in the present case to a zero range pseudopotential $\hat{J}_{00} \delta(\mathbf{s})$, with a strength depending slightly on the energy. We have used the common prescription [22] $\hat{J}_{00} = -276 \text{ MeV fm}^3$ neglecting completely the small energy dependence. For example, the odd-even staggering in the Q -value for a fragmentation channel, which is typically of the order $\Delta Q = 2 \text{ MeV}$, leads to a variation with $\Delta \hat{J}_{00} = -0.005 \Delta Q / \mu \text{ MeV} \cdot \text{fm}^3$ with $\mu \approx 100$. The one-body densities in (1) are taken as Fermi distributions in the intrinsic frame

$$\rho(\mathbf{r}) = \frac{\rho_0}{1 + e^{\frac{r-c}{a}}} \quad (2)$$

with $c = c_0(1 + \sum_{\lambda \geq 2} \beta_\lambda Y_{\lambda 0}(\Omega))$. Only static axial symmetric deformations are considered. The half radius c_0 and the diffusivity are taken either from liquid drop model [27] or from the spherical HF calculations [23]. The normalization constant ρ_0 is determined by requiring the particle number conservation

$$\int r^2 dr d\Omega \rho(r, \Omega) = A \quad (3)$$

and then the multipoles are computed numerically

$$\rho_\lambda(r) = \int d\Omega \rho(r, \Omega) Y_{\lambda 0}(\Omega). \quad (4)$$

Once the multipole expansion of the density is obtained, the integral in (1) becomes

$$V_F(\mathbf{R}, \omega_1, \omega_2) = \sum_{\lambda_1 \mu_1 \lambda_2 \mu_2} D_{\mu_1 0}^{\lambda_1}(\omega_1) D_{\mu_2 0}^{\lambda_2}(\omega_2) I_{\lambda_1 \mu_1 \lambda_2 \mu_2} \quad (5)$$

where [24,25]

$$I_{\lambda_1 \mu_1 \lambda_2 \mu_2} = \sum_{\lambda_3 \mu_3} B_{\lambda_1 \mu_1 \lambda_2 \mu_2}^{\lambda_3 \mu_3} \int r_1^2 dr_1 r_2^2 dr_2 \rho_{\lambda_1}(r_1) \rho_{\lambda_2}(r_2) F_{\lambda_1 \lambda_2 \lambda_3}^v(r_1, r_2, R) \quad (6)$$

and

$$F_{\lambda_1 \lambda_2 \lambda_3}^v(r_1, r_2, R) = \int q^2 dq \tilde{v}(q) j_{\lambda_1}(qr_1) j_{\lambda_2}(qr_2) j_{\lambda_3}(qr_3). \quad (7)$$

Above, $D_{\mu 0}^\lambda(\omega)$ stands for Wigner rotation matrix describing the orientation ω of the intrinsic symmetry axis with respect to the fixed frame, $\tilde{v}(q)$ denotes the Fourier transform of the interaction and j_λ are spherical Bessel functions. The matrix B in (6) is defined in [24] and contains selection rules for coupling angular momenta. For example only $\lambda_1 + \lambda_2 + \lambda_3 = \text{even}$, are allowed. When $\beta_\lambda \neq 0$, $\lambda = 2, 3, 4$ for both fragments, then the sum in (5) involves 32 terms for a nose-to-nose configuration and $\lambda_3 \leq 6$. Special care has been payed to obtain numerically the integrals involved in expressions (4) and (6-7). For most of the fragmentation channels studied here, large quadrupole, hexadecupole, and occasionally octupole deformations are involved. Therefore a Taylor expansion method for obtaining the density multipoles cannot be considered. On the other hand, a large quadrupole

deformation induces according to (4) nonvanishing multipoles with $\lambda=4$ and 6 even if $\beta_4=\beta_6=0$. Therefore for a correct calculation of (4), a numerical method with a truncation error of order $O(h^7)$ is needed in order to ensure the orthogonality of spherical harmonics with $\lambda \leq 6$.

Performing the integrals (6) and (7) we have used a numerical method with a truncation error of the order $O(h^9)$. All short range wavelength ($q \leq 10 \text{ fm}^{-1}$) have been included and particular care has been taken to ensure the convergence of the integrals with respect to the integration step and the range of integration.

The asymptotic part of the barrier is determined essentially by the Coulomb multipoles which are obtained also as double folding integrals involving charge densities. For $R \gg r_1 + r_2$, the Coulomb kernel in (7) behaves as [24]

$$F_{\lambda_1\lambda_2\lambda_3}^C(r_1, r_2, R) = 2\pi^2 \frac{(2\lambda_3 + 1)!!}{(2\lambda_3 + 1)(2\lambda_1 + 1)!!(2\lambda_2 + 1)!!} \frac{r_1^{\lambda_1} r_2^{\lambda_2}}{R^{\lambda_3+1}} \delta_{\lambda_3, \lambda_1 + \lambda_2}. \quad (8)$$

If we introduce the moments of the charge density as

$$Q_\lambda = \sqrt{\frac{4\pi}{2\lambda + 1}} \int_0^\infty r^2 dr \rho_\lambda(r) r^\lambda \quad (9)$$

where $Q_0 = Z$ (atomic number) then the $\lambda_3 = 2$ component of function (6) behaves for $R \rightarrow \infty$ as

$$(C_{000}^{202})^2 \frac{Z^1 Q_2^2 + Z^2 Q_2^1}{R^3}. \quad (10)$$

At the scission configuration we assumed two coaxial deformed fragments in contact at their tips. For quadrupole deformations we choose two coaxial prolate spheroids due to the fact that the prolate shapes are favoured in fission. It is known that for each oblate minimum always corresponds another prolate minimum. For pear shapes, i.e. fragments with quadrupole and octupole deformations, we choose opposite signs for the octupole deformations, i.e. nose-to-nose configurations (see Fig.1). For hexadecupole deformations we choose only positive signature, because it leads to a lowering of the barriers in comparison with negative ones and consequently they are much more favoured in fission (see Fig.2).

In order to illustrate the influence of deformations on the barriers we displayed in Fig.3 the M3Y-folding multipoles for ^{98}Sr and ^{144}Ba with all deformations included. The octupole component is large in the interior but gives negligible contribution in the barrier region in contrast with the hexadecupole one. Next, in Fig.4 we are illustrating for the same partners the cumulative effect of high rank multipoles on the barrier. We stress the correct asymptotic behaviour of multipoles, especially of the component $\lambda_3 = 2$ of function (6) given by expression (10) which survives up to very large distances if the quadrupole deformation is large.

3. Isotopic Yields with Liquid Drop Parameters

We should like to stress again that in our simple cluster model we neglect the preformation factors for different channels, i.e. we use the same frequency factor ν for the collisions with the fission barrier for all fragmentations. It is generally known that the general trends in alpha decay of heavy nuclei are very well described by barrier penetrabilities, the preformation factors becoming increasingly important only in the vicinity of the double magic nucleus ^{208}Pb . On the other hand the cold binary fragmentation of ^{252}Cf was also reasonably well described using constant preformation factors [6,28]. Similarly we expect that the ternary cold splittings could be described in the first order approximation only by the barrier penetrabilities. Eventually, as the experimental data become more accurate we would be able to extract some fragment preformation factors and discuss the related nuclear structure effects. Presently, it is too early to compute cluster preformation factors on the nuclear surface of a fissioning nucleus [29].

In the laboratory frame of reference the z -axis was taken as the initial fissioning axis of the two heavier fragments, with the origin at their point of contact. We assumed that the three bodies are moving in the (z, x) plane. The potential barriers $V_{HL} - Q_{HL}$ between the two fragments are high but rather thin with a width of about 2 to 3 fm. As an illustration, we show in Fig.5 a typical barrier between ^{142}Xe and ^{100}Zr , as a function of the distance R_{HL} between their center of mass. Here $Q_{HL} = Q_t - Q_c$ is the decay energy for binary fragmentation (in our case that of ^{242}Pu) and $Q_c = 8.71$ MeV is the ^{10}Be decay energy from ^{252}Cf .

On the other hand the LCP is initially situated in the potential well which is created by the sum of the potentials between the LCP and the two heavier fragments. As an illustration we present in Fig.6 this potential barrier for the light cluster, as a function of its position in the (z, x) plane, at three different values of the inter-fragment distance R_{HL} . The corresponding ternary splitting is the same as in Fig. 5. We can see that as the distance between the two heavier fragments increases the LCP potential well is narrowing and its bottom rises, forcing the cluster to jump over the barrier and to be repelled along the x -axis by the Coulomb field of the other two fragments. For the two fragments, the exit point from their potential barrier is at R_{HL} typically between 15 and 16 fm (see Fig.5) which supports our cluster model. Evidently from the top of the cluster barrier we can compute the classical trajectories of the three fragments as a function of time.

Due to the fact that the barrier between the two heavier fragments is much thinner than the barrier between the LCP and the heavier fragments, in our model first the two heavier fragments penetrate the potential barrier between them and later-on the LCP is emitted. In such a model the mass distributions of the heavier fragments are not influenced by the cluster trajectories. Consequently these mass distributions are very similar to that of the cold binary fission of an initial nucleus leading to the same heavier fragments, i.e. in our case ^{242}Pu . This mechanism is supported by the comparison between the experimental data concerning the fission mass distributions in binary and alpha-accompanied fission of ^{235}U [30]. From these

data the experimentalists concluded that the LCP is preferentially emitted by the light fragment [14]. We should like to mention that a sequential emission of a ^{10}Be cluster from the already separated fragments is not possible due to the fact that these are very neutron-rich nuclei with negative or close to zero Q values. In addition, the presence of a Coulomb barrier further hinders LCP emissions from the heavier fragments in comparison with the neutron evaporation process at excitation energies above 6-7 MeV. On the other hand, it is known that for the mass distributions in asymmetric spontaneous fission of the lighter actinides compared to the heavier ones, the position of the heavy mass peak remains unchanged while the light mass peak moves to lower A_L values [14,30]. Thus from our model we conclude that the mass distribution of fission fragments in cold ternary fission is almost identical with the mass distribution for the cold binary fission of the daughter nucleus (i.e. the initial nucleus from which the LCP was extracted). This looks like the LCP was emitted from the light fragment.

The penetrabilities through the double-folded potential barrier between the two heavier fragments were calculated by using the WKB approximation

$$P = \exp \left\{ -\frac{2}{\hbar} \int_{s_i}^{s_o} \sqrt{2\mu [V_{HL}(s) - Q_{HL}]} ds \right\} \quad (11)$$

where s is the relative distance, μ is the reduced mass and s_i and s_o are the inner and outer turning points, defined by $V_{HL}(s_i) = V_{HL}(s_o) = Q_{HL}$.

The barriers were computed with the LDM parameters $a_p = a_n = 0.5$ fm, $r_{0p} = r_{0n} = (R - 1/R)A^{-1/3}$ fm with $R = 1.28A^{1/3} + 0.8A^{-1/3} - 0.76$.

Accurate knowledge of Q values is crucial for the calculation, since the WKB penetrabilities are very sensitive to them. We obtained the Q values from experimental mass tables [26], and for only a few of the fragmentations the nuclear masses were taken from the extended tables of Möller et al. [27] computed using a macroscopic-microscopic model.

In this paragraph we consider only the relative isotopic yields corresponding to true cold (neutronless) ternary fragmentations in which all final nuclei are left in their ground state. These ternary relative isotopic yields are given by the expression ($A_1 = A_L, A_2 = A_H$)

$$Y(A_1, Z_1) = \frac{P(A_1, Z_1)}{\sum_{A_1 Z_1} P(A_1, Z_1)} \quad (12)$$

As fragment deformations we choose the ground state deformations of Möller et al. [27] computed in the frame of the macroscopic-microscopic model. Due to the fact that the influence of fragment deformations on barrier penetrabilities, i.e. on ternary yields, is extremely large we represented in Fig.7 these deformations for the light A_1 and heavy A_2 fragments, separately for odd and even charge Z . We can see that the light fragments, have mainly quadrupole deformations in contrast with the heavy fragments, which have all deformations. The octupole deformations are existing for a small heavy fragment mass number region $141 \leq A_2 \leq 148$. The fragments with mass number $A_L \leq 92$ and $A_H \leq 138$ are practically spherical.

The computed M3Y-fission barriers heights, for different assumptions: no deformations, including the quadrupole ones, including the quadrupole and octupole ones and for all deformations, together with the corresponding Q -values are represented in Fig.8 for odd Z and even Z separately. We can see that the largest influence is due to the quadrupole deformations but also the hexadecupole ones are lowering the barriers very much. A strong lowering of barriers height starts around $A_1 = 95$, $A_2 = 139$ and finish at $Z_1 = 41$, $A_1 = 104$ and $Z_1 = 42$, $A_1 = 103$ which corresponds to the sudden increase of deformations for $Z_2 = 53$, $A_2 = 138$ and $Z_2 = 52$, $A_2 = 139$ (Fig.7). The octupole deformations in the mass region $141 \leq A_2 \leq 148$ have a smaller effect as we expect. This is a illustration of the difference between cluster radioactivity, which is due only to the large Q -values and the cold fission which is due mainly to the lowering of the barriers due to the fragment deformations. Both processes are cold fragmentation phenomena.

The computed yields in percents, for the splittings represented by their fragment deformation parameters in Fig.7, or by their barrier heights in Fig.8 are given in Fig.9 for spherical fragments ($\beta = 0$), for quadrupole deformations (β_2) and for all deformations ($\beta_2 + \beta_3 + \beta_4$). We can see that for spherical fragments the splittings with the highest Q -values, which correspond to real spherical heavy fragments(see Fig.7), i.e. for charge combinations $Z_1/Z_2 = 44/50$, $43/51$ and $42/52$ are the predominant ones. As we mentioned before this situation is similar with the cluster radioactivity were the main fact is the Q -value. Due to the staggering of Q -values(see Fig.8) the highest yields are for even-even splittings. By including the β_2 deformations few asymmetric splittings exists. For all deformations more asymmetric yields appear. Now the principal yields are for $Z_1/Z_2 = 38/56$ and $40/54$. This is due to the fact that the influence of the fragment deformations on the yields could compensate the influence of Q -values. This illustrate the fact that cold fission is a cold rearrangement process in which all deformations are playing the main role and not the Q -values. The staggering for odd Z fragmentations like $Z_1/Z_2 = 39/55$, $41/53$ and $43/51$ or odd N fragmentations is recognized at first glance. We shall see later on that by the introduction of the density levels this staggering is reversed. The largest yields will be for odd Z and/or N fragmentations.

In the next figures, we represented the mass yields $Y_{A_1} = \sum_{Z_1} Y(A_1, Z_1)$ (Fig.10) and the charge yields $Y_{Z_1} = \sum_{A_1} Y(A_1, Z_1)$ (Fig.11) for spherical fragments ($\beta_i=0$), for quadrupole ($\beta_2 \neq 0$) ones and for all deformations ($\beta_i \neq 0$). We can see that for spherical fragments the main mass yields are $A_1=108$, 110 and 112 for spherical or for prolate shapes. The hexadecupole deformations shifts the main yields to $A_1=96-104$. The experiment will decide if these deformations are participating to the cold fission process. We stress the odd-even mass and charge staggering which already existed at individual yields $Y(A_1, Z_1)$.

These predictions are very useful as a first guide for unfolding the cold ternary yields from the very complex experimental gamma-ray spectra containing the contributions from over 100 fission fragments. We should like to stress the correlation between the ternary fission Q_t values and the isotopic yields. Usually for a given mass fragmentation the highest yield corresponds to the charge splitting with the highest Q_t value, but in a few cases where the fragment deformations are large,

this correspondence is reversed. This support our interpretation of cold fission as cluster radioactivity.

4. Isotopic yields with Hartree-Fock parameters

In order to obtain the parameters of the one-body densities involved in the folding integral, we have performed a large scale (162 nuclei) standard spherical Hartree-Fock(HF) calculation using the energy density formalism of Beiner and Lombard [23]. The functional F_1 was used for all nuclei since it reproduces correctly the bulk properties of spherical nuclei (binding, separation energies, single particle levels, charge radii, etc.). The shell model occupation probabilities were used in constructing the single particle orbitals. Pairing interactions were neglected. This is a limitation in our calculation. However this type of correlations are implicitly included in our densities since we used the deformations given by the macroscopic-microscopic model of Möller et al.[27]. For each nucleus considered, the HF density was fitted with a Fermi distribution in the range 2-18 fm. We obtained good quality fits in the surface region which largely determines the diffusivity. The fitting parameters (reduced radii and diffusivities) were displayed in Fig.12 which clearly emphasize the effect of partial filling of nuclear subshells. In Fig.13 we represented the barrier heights for different assumptions on fragment deformations : spherical, prolate, pear-shape and with hexadecupole as a function of the light fragment mass. We see the same strong dependence of barriers heights on the fragment deformations like in the case of liquid drop model parameters(Fig.9). In Fig.14 we give the cold fission yields in percents for zero fragment deformations, with quadrupole and with all deformations included. In order to understand the behaviour of HF-parameters we represented in Fig.15: the inner turning point (r_1) the outer turning point (r_2), the radius at the barrier height (r_b) and the radius of the touching configurations $r_t = (r_{A_1}^2)^{1/2} + (r_{A_2}^2)^{1/2}$ as a function of the light fragment mass. We stress that r_t is a smooth function of A_1 , while r_1 and r_b are strongly influenced by deformations and r_2 reflects the odd-even staggering of Q -values.

In Fig.16 we represented the mass yields $Y_A = \sum_Z Y(Z, A)$ and in Fig.17 the charge yields. The general behaviour is similar with the trend given by the yields computed with the liquid drop model parameters (see Figs.10,11). The geometrical parameters of the one-body densities (reduced radius and diffusivity), provided they have realistic values, influences to a lesser extent the relative yields, as compared with Q -values and deformation parameters.

5. Ternary yields as Function of Fragment Excitation Energy

In the following we shall study the influence of the level density and of the total excitation energy (TXE) of the fragments on ternary yields.

Following a suggestion of Schwab et al. [3] we define the level density for the composite system as a function of total excitation energy (TXE)

$$\rho(TXE) = \int_0^{TXE} \rho_L(e)\rho_H(TXE - e)de \quad . \quad (13)$$

where $\rho_{L(H)}$ are the individual level densities of the fragments. The above definition is consistent with the hypothesis of a uniform distribution of the total available excitation energy between the fragments. For excitation energies larger than 1MeV we have used the usual formula obtained within the Back Shifted Fermi Gas Model(BSFGM).

The level density parameter and the fictious ground state position (a and Δ respectively) were taken from the global analysis of Dilg et al.[31]. For smaller excitation energies the BSFGM level density was smoothly joined with a formula by Grossjean and Feldmayer [32] which avoids a singularity close to $e \rightarrow 0$. We should like to mention that the introduction of a fictious ground state position, according to odd -even Z or N , change completely the odd-even effect in Z or N . If before the even-even splittings were favoured, now the largest yields are for odd-odd Z or/and N splittings in agreement with the experimental data.

Second, we shall consider the change of deformation due to the fragment excitation energy. Like in our previous papers [28,33] we assume that the total excitation energy $TXE = Q - TKE$ will lead to a supplementary deformation of the fragments viewed as a β -stretching along the elongation axis. According to this model at the scission point the fragments will have slightly bigger defformations than the ground state values. The excitation energy TXE is supposed to be divided proportionaly to the mass of each fragment, i.e. $E_i^* = \frac{A_i}{A_1+A_2}TXE$ ($i = 1, 2$). Then the *induced* deformation coming-up from the β -polarization of fragment i is given by the expression [28]:

$$\beta(E^*) = \left\{ \beta_0^2 + \frac{\hbar}{2B\omega_\beta} \left(\frac{2E^*}{\hbar\omega_\beta} + 1 \right) \right\}^{1/2} \quad (14)$$

where β_0 is the ground state deformation of the corresponding fragment, B is the mass parameter and ω_β is the frequency for the β -vibrations, both being evaluated from the experimental data. The use of the β -stretching is motivated by the fact that the cold fission yields are increasing with the excitation energy [1,3,8]. The level density is also increasing, but not enough to compensate the decrease of the barrier penetrabilities with the increase of the excitation energy. Consequently by β -stretching we increase the deformations, i.e. we decrease the barriers which leads to the increase of the barrier penetrabilities which allows to reproduce such a trend of cold fission yields. In a previous paper [33] we succeeded to describe excellently the behaviour of the experimental cold fission yields for the thermal neutron fission of ^{233}U as a function of the excitation energy.

We would like to stress that according to expression (14) the excitation energy will enhance the deformations especially for fragments with large deformations. On the other hand in cold fission the two fragments must have a stretched out scission

configuration in order to have a large penetrability, i.e. large yield. Consequently only the combinations for which the increase of deformations is large enough are observed experimentally. This may change the order of fragmentation channels which are mainly contributing to a given isotopic yield.

The penetrabilities computed with β -stretching multiplied with the level density for excitation energies $E^*=1, 3$ and 5 MeV are represented in Fig.18. We can see that more combinations are contributing to the cold fission yields with the increase of the excitation energy. Only a detailed comparison with the experimental data will give an answer if the present dynamical model describe correctly the experimental data. Obviously the level densities fitted for the outer region with neutron rich fragments and the introduction of other types of polarizations are necessary.

6. Experiments

Up to now, in order to study the binary and alpha ternary fission of ^{252}Cf , a source of strength $\sim 6 \times 10^4$ fissions/s, sandwiched between two Ni foils of thickness 0.5 mil and then sandwiched between 2 mil thick Al foils, was placed at the center of the Gammasphere with 72 Compton suppressed Ge detectors. A total of 9.8×10^9 triple or higher fold coincidence events were recorded. A $\gamma - \gamma - \gamma$ "coincidence cube" was built using the RADWARE software program [34]. In the fission of ^{252}Cf , about 100 different final fragments are produced. First, these primary fragments emit several neutrons until the excitation energy of the fragment is below the neutron binding energy (~ 6 MeV). The excited primary fragments are too neutron-rich to emit charged particles such as protons, alpha particles or light charge particles as ^{10}Be . Then, the secondary fragments decay to their ground states by the emission of γ -rays. Only the correlations between the two heavier fragments were observed unambiguously by using the triple-gamma coincidence.

The neutron multiplicities and the correlated yields of Z secondary binary fragments were determined by setting a double gate on the light fragment and measuring the gamma intensities in the heavy fragment with different number of evaporated neutrons. For the odd-odd fragmentations we considered the total intensities obtained from summing all the gamma transitions to the ground state. Correcting the number of counts for the detector efficiency and for internal conversion, we obtain the gamma transition relative yields for the different neutron channels. Then the sum of these ground state transition yields are normalized, for a given light fragment, to the Wahl Tables which give the estimated total isotopic yields in the binary fission of ^{252}Cf [35]. If one isotope from the heavy fragment is missing we evaluate its corresponding yield by interpolation from its neighbors with a Gaussian. A cross-check is necessary by imposing a double gate on the heavy fragment and determining the gamma intensities of the corresponding correlated light fragments. Again the sum of these yields are normalized to the Wahl

Tables [35] for the heavy fragment. The final isotopic yields must be consistent. In cases where either the background is large or when the gates are complex because of multiple γ -rays of the same energies a third determination was made by setting a gate on the light fragment and another gate on the heavy fragment. Determining the intensities in both fragments and knowing the branching ratios between different transitions we can determine again the binary yields [5,6]. We should like to mention that presently the spectra of odd- Z nuclei are not known, which does not allow us to determine experimentally the odd- Z isotopic yields.

The cold (neutronless) binary yield represents only 0.2% from the total fission yield. Due to the fact that the values of the alpha ternary yields are comparable with the values of cold binary yields the background must be similar [36].

The ^{10}Be -ternary yields are at least 100 times smaller than α -ternary yields, i.e. 0.002% [37]. For the corresponding cold yields we expect the same ratio. Consequently we have to be very careful with the accidental coincidence of the two final fragments with their binary partners. The detection of fragments by particle detectors in coincidence with the γ -rays of the fragments does not solve this problem. The binary partners of the fragments will be present by their characteristic γ -rays. Any how the large background will be reduced. At least, due to the fact that we could detect the TKE of the fragments, we can determine the yields as function of fragment TKE . Another possibility is to detect directly the ^{10}Be -nucleus by a particle detector. Unfortunately the large background of alpha particles will cover such a small yield. A much more reasonable possibility look like to use a characteristic γ -ray of ^{10}Be in coincidence with the fragments of γ -rays. This will eliminate the large background due to the binary partners of the fragments.

We should stress here that up to now the experimentally determined isotopic yields by triple γ -coincidence method are integrated yields. In the spontaneous fission experiment of ^{252}Cf the majority of the binary and ternary splittings lead to highly excited final nuclei which after neutron evaporation are decaying to the lowest states by gamma cascades. Less frequently, there are cold fragmentations which leave the final nuclei in their ground or first excited states. We define these cold fission experimental yields as integrated yields since they collect the contributions of all (neutronless) transitions over a whole range of TXE from zero up to at least the neutron binding energy, from where the evaporation of a first neutron becomes possible. For a deeper interpretation we need the yields as a function of the excitation energy of fragments.

7. Discussions and Conclusions

The cold alpha ternary fission of a heavy nucleus (^{252}Cf) was experimentally recently observed directly for the first time [36]. Some indications of ^{10}Be and ^{14}C ternary fragmentations were also obtained [19,20]. The cold ternary fission events are characterized by very low TXE of the final fragments and high TKE tending to the Q_t value associated to those splittings. Thus the configuration

at the scission point should be described in these cases by very compact shapes, the deformed fragments in their ground states. It was already shown that for cold binary fragmentations, the ground state deformations are a key ingredient for the correct prediction of the most favoured splittings and of the isotopic yields [6,17,18,28]. The cluster model which we used in this paper for calculating the isotopic yields associated with ^{10}Be -accompanied cold ternary fission, also predicts a large number of favored ternary splittings in which one or both heavier fragments are well deformed in their ground states.

The determination of the scission point configurations in the fission of heavy nuclei starting from the experimental kinetic energy and angular distributions of the LCP emitted in ternary fission, has been a great hope for many years. Unfortunately too many unknown parameters are associated with the initial scission point configurations in the case of the usual "hot" ternary fission. But for cold ternary fission the initial scission configurations are known : the fragment deformations should be essentially that of the ground state deformations. Of course the initial position and velocity distributions of the LCP have to be determined from their final kinetic energy and angular distributions.

Presently the spontaneous cold fission of three nuclides, namely ^{252}Cf , ^{248}Cm and ^{242}Pu , is under study using the triple gamma coincidence technique. The same set of deformation parameters should explain the cold binary fission yields in all three cases so that we expect to extract new experimental information over different nuclear deformation regions. In addition the cold alpha ternary fission yields of ^{252}Cf should be similar to the cold binary fission yields of ^{248}Cm [21] and the cold ^{10}Be - ternary fission yields of the same parent nucleus should be similar to the cold binary fission yields of ^{242}Pu [38,39]. Consequently many cross-checks are possible. In addition the kinetic energies and angular distributions of light clusters emitted in cold ternary fission will provide new important insight on the fragmentation processes of heavy nuclei.

Acknowledgements.

The work at Vanderbilt University was supported in part by the U.S. Department of Energy under grant No. DE-FG05-88ER40407. The Joint Institute for Heavy Ion Research has member institutions the University of Tennessee, Vanderbilt University and Oak Ridge National Laboratory. It is supported by its members and by the U.S. Department of Energy through contract No. DE-FG05-87ER40361 with the University of Tennessee. A.S., F.C., Ş.M. would like to acknowledge the hospitality of Gessellschaft für Schwerionenforschung, Darmstadt, Germany, and A.S. and A.F. of Vanderbilt University, Nashville, U.S.A. during the completion of this work. We would like to acknowledge the grant received under Twinning Program from National Research Council.

References

- [1] F.-J. Hamsch, H.-H. Knitter and C. Budtz-Jorgensen, Nucl. Phys. **A554**, 209 (1993).
- [2] A. Benoufella, G. Barreau, M. Asghar, P. Audouard, F. Brisard, T.P. Doan, M. Hussonnois, B. Leroux, J. Trochon and M.S. Moore, Nucl. Phys. **A565**, 563 (1993).
- [3] W. Schwab, H.-G. Clerc, M. Mutterer, J.P. Theobald and H. Faust, Nucl. Phys. **A577**, 674 (1994).
- [4] J.H. Hamilton, A.V. Ramayya, J. Kormicki, W.C. Ma, Q. Lu, D. Shi, J.K. Deng, S.J. Zhu, A. Săndulescu, W. Greiner, G.M. Ter-Akopian, Yu.Ts. Oganessian, G.S. Popeko, A.V. Daniel, J. Kliman, V. Polhorsky, M. Morhac, J.D. Cole, R. Aryaeinejad, I.Y. Lee, N.R. Johnson and F.K. McGowan, J. Phys. G: Nucl. Part. Phys. **20**, L85 (1994).
- [5] G.M. Ter-Akopian, J.H. Hamilton, Yu.Ts. Oganessian, J. Kormicki, G.S. Popeko, A.V. Daniel, A.V. Ramayya, Q. Lu, K. Butler-Moore, W.C. Ma, J.K. Deng, D. Shi, J. Kliman, V. Polhorsky, M. Morhac, W. Greiner, A. Săndulescu, J.D. Cole, R. Aryaeinejad, N.R. Johnson, I.Y. Lee and F.K. McGowan, Phys. Rev. Lett. **73**, 1477 (1994).
- [6] A. Săndulescu, A. Florescu, F. Cârstoiu, W. Greiner, J.H. Hamilton, A.V. Ramayya and B.R.S. Babu, Phys. Rev. **C 54**, 258 (1996).
- [7] E.R. Hulet, J.F. Wild, R.J. Dougan, R.W. Loughheed, J.H. Landrum, A.D. Dougan, M. Schadel, R.L. Hahn, P.A. Baisden, C.M. Henderson, R.J. Dypzyk, K. Summerer and G.R. Bethune, Phys. Rev. Lett. **56**, 313 (1986).
- [8] A.Möller, M.Crönni, F.Gönnenwein, G.Petrov, Int.Conference on Large Scale Collective Motion of Atomic Nuclei, Brolo, 1996
- [9] A. Săndulescu and W. Greiner, Rep. Progr. Phys. **55**, 1423 (1992).
- [10] P.B. Price, Nucl. Phys. **A502**, 41c (1989).
- [11] A. Săndulescu and W. Greiner, J. Phys. G : Nucl. Phys. **3**, L189 (1977).
- [12] A.Săndulescu, J. Phys. G : Nucl. Part. Phys. **15**, 529 (1989).
- [13] R. Vandenbosch and J. Huizenga, Nuclear Fission, Academic Press, New York, 1973.
- [14] C. Wagemans, Ternary Fission, in: The Nuclear Fission Process, Ed. C. Wagemans, CRC Press, Boca Raton FL, 1991.

- [15] F. Gönnerwein, B. Borsig, U. Nast-Linke, S. Neumaier, M. Mutterer, J.P. Theobald, H. Faust and P. Geltenbort, 6-th Int. Conf. on Nuclei Far from Stability and 9-th Int. Conf. on Atomic Masses and Fundamental Constants, Bernkastel-Kue 1989, p.453.
- [16] J.F. Wild, P.A. Baisden, R.J. Dougan, E.K. Hulet, R.W. Loughheed and J.H. Landrum, Phys. Rev. C **32**, 488 (1985).
- [17] A. Săndulescu, A. Florescu and W. Greiner, J. Phys. G: Nucl. Part.Phys. **15**, 1815 (1989).
- [18] F. Gönnerwein and B. Borsig, Nucl. Phys. **A530**, 27 (1991).
- [19] A.V. Ramayya, J.H. Hamilton, J.K. Hwang, J. Kormicki, B.R.S. Babu, A. Florescu, A. Săndulescu, F. Cârstoiu, W. Greiner, J.D. Cole, R. Aryaeinejad, Y.X. Dardenne, K. Butler-Moore, M.K. Drigert, W.C. Ma, G.M. Ter-Akopian, Yu.Ts. Oganessian, A.V. Daniel, J.O Rasmussen, S.J. Asztalos, I.Y. Lee, A.O. Machiavelli, M.A. Stoyer, R.W. Loughheed, J.F. Wild and S.G. Prussin, Third Int. Conf. on Dynamical Aspects of Nuclear Fission (August 30- September 4) 1996, Casta-Papiernicka, Slovak Republic.
- [20] A.V. Ramayya, J.H. Hamilton, J.K. Hwang, J. Kormicki, B.R.S. Babu, A. Florescu, A. Săndulescu, F. Cârstoiu, W. Greiner, J.D. Cole, R. Aryaeinejad, Y.X. Dardenne, K. Butler-Moore, M.K. Drigert, W.C. Ma, G.M. Ter-Akopian, Yu.Ts. Oganessian, A.V. Daniel, J.O Rasmussen, S.J. Asztalos, I.Y. Lee, A.O. Machiavelli, M.A. Stoyer, R.W. Loughheed, J.F. Wild and S.G. Prussin, Int. Research Workshop on Heavy Ion Physics at Low, Intermediate and Relativistic Energies using 4π Detectors, Poiana Braşov (October 7-14) 1996, Romania.
- [21] A. Săndulescu, A. Florescu, F. Cârstoiu and W. Greiner, J. Phys. G : Nucl. Part. Phys. **22**, L87 (1996).
- [22] M.E. Brandan, G.R. Satchler , Phys. Rep. **285**, 143 (1997).
- [23] M. Beiner and R.J. Lombard, Ann.Phys. **86**, 262 (1974).
- [24] F. Cârstoiu and R.J. Lombard, Ann. Phys. (N.Y.) **217**, 279 (1992).
- [25] A. Săndulescu, R.K. Gupta, W. Greiner, F. Cârstoiu and M. Horoi, Int. J. Mod. Phys. **E 1**, 379 (1992).
- [26] A.H. Wapstra, G. Audi and R. Hoeckstra, At. Data Nucl. Data Tables **39**, 281 (1988).
- [27] P. Möller, J.R. Nix, W.D. Myers and W.J. Swiatecki, At. Data Nucl. Data Tables **59**, 185 (1995).
- [28] A. Florescu, A. Săndulescu, C. Cioacă and W. Greiner, J. Phys. G: Nucl. Part. Phys. **19**, 669 (1993).

- [29] N. Cârjan, A. Săndulescu and V.V. Pashkevich, Phys. Rev. **C 11**, 782 (1975).
- [30] J.P. Theobald, Report IKDA 85/22, Technische Hochschule Darmstadt, FRG, 1985.
- [31] W. Dilg, W. Schantl, H. Vonach and M. Uhl, Nucl.Phys. **A217**, 269(1973).
- [32] M.K. Grossjean and H. Feldmeier, Nucl.Phys. **A444**, 113(1985).
- [33] V. Avrigeanu, A. Florescu, A. Săndulescu and W. Greiner, Phys.Rev. **C 52**, 1755(1995).
- [34] D.C. Radford, Nucl. Instr. Meth. Phys. Res., **A361**, 297 (1995).
- [35] A.C. Wahl, At. Data Nucl. Data Tables **39**, 1 (1988).
- [36] A.V. Ramayya, J.H. Hamilton, J.K. Hwang, L.A. Peker, J. Kormicki, B.R.S. Babu, T.N. Ginter, A. Săndulescu, A. Florescu, F. Cârstoiu, W. Greiner, G.M. Ter-Akopian, Yu.Ts. Oganessian, A.V.Daniel, W.-C. Ma, P.G. Varmette, J.O. Rasmussen, S.J. Asztalos, S.Y. Chu, K.E. Gregorich, A.O.Machiavelli, R.W.Macleod, J.D.Cole, R. Aryaeinejad, K. Butler-Moore, M.W. Drigert, M.A.Stoyer, L.A.Bernstein, R.W.Longheed, S.G.Prussin, S.J.Zhu, H.C. Griffin, R. Donangelo, Phys.Rev.**C** (to be published).
- [37] A. Săndulescu, A. Florescu, F. Cârstoiu, A.V. Ramayya, J.H. Hamilton, J.K. Hwang, B.R.S. Babu, and W. Greiner, Phys.Rev. **C** (to be published).
- [38] J.H. Hamilton, A.V. Ramayya, S.J. Zhu, G.M. Ter-Akopian, Yu.Ts. Oganessian, J.D. Cole, J.O. Rasmussen and M.A. Stoyer, Prog. Part. Nucl. Phys. **35**, 635 (1995).
- [39] Y.X. Dardenne, R. Aryaeinejad, S.J. Asztalos, B.R.S. Babu, K. Butler-Moore, S.Y. Chu, J.D. Cole, M.W. Drigert, K.E. Gregorich, J.H. Hamilton, J. Kormicki, I.Y. Lee, R.W. Loughheed, Q.H. Lu, W.-C. Ma, M.F. Mohar, K.J. Moody, S.G. Prussin, A.V. Ramayya, J.O. Rasmussen, M.A. Stoyer and J.F. Wild, Phys Rev. **C 54**, 206 (1996).

Figure Captions

Fig. 1. Density plots of ^{98}Sr and ^{144}Ba fragments, placed at $R=15\text{fm}$, considered with quadrupole and octupole deformations. In the upper part are represented the prolate-prolate, oblate-prolate positions and in the lower part two pear shapes nose to back and nose to nose. The positions are given by the deformation signs.

Fig. 2. Same as for Fig.1. The influence of different signs of hexadecupole deformations on ^{98}Sr and ^{144}Ba densities in the presence of large quadrupole and octupole deformations. The penetrability is maximized for $\beta_4 > 0$ configurations.

Fig. 3. The influence of the M3Y-folding multipoles on the barrier between ^{98}Sr and ^{144}Ba . Notice that the main effect is due to $\lambda_3 = 2$. The influence of $\lambda_3 = 3$ is large but less important in the barrier region compared with the induced deformations $\lambda_3 = 5$ and $\lambda_3 = 6$.

Fig. 4. The cumulative effect of high rank multipoles on the barrier between ^{98}Sr and ^{144}Ba . We considered the deformations β_3 and β_4 much larger than the real ones in order to illustrate the effect of deformations.

Fig. 5. The barrier between ^{142}Xe and ^{100}Zr as a function of the distance R_{HL} between their centers of mass. By $Q_{HL} = Q_t - Q_c$ we denote the decay energy of daughter nucleus (^{242}Pu) where Q_t is the ternary decay energy for ^{10}Be ternary cold splitting and $Q_c=8.71\text{MeV}$ is the ^{10}Be decay energy from ^{252}Cf .

Fig. 6. The barrier between the ^{10}Be cluster and the two heavier fragments in the (z, x) plane for three fixed distances between them : (a) $R_{HL} = 12.6$, (b) $R_{HL} = 16.6$ and (c) $R_{HL} = 20.6$. Note the larger cluster barrier widths.

Fig. 7. The assumed $\beta_2, \beta_3, \beta_4$ ground state fragment deformations [27]. We can see that the light fragments (Z_1, A_1) have mainly quadrupole deformations in contrast with the heavy fragments (Z_2, A_2). The octupole deformations are existing in a small mass region $141 \leq A_2 \leq 148$. The fragments with masses $A_1 \leq 90$ and $A_2 \leq 138$ are practically spherical.

Fig. 8. The barrier heights for all considered fragmentations channels represented for different charges Z_1 and mass numbers A_1 of the light fragment. The

strong lowering of the barrier heights at $Z_1=41$, $A_1=104$ and $Z_1=42$, $A_1=103$ corresponds to the sudden increase of deformations at $Z_2=53$, $A_2=138$ and $Z_2=52$, $A_2=139$ (Fig.7). The decrease of barrier heights starts approximately at $A_1=95$, respectively at $A_2=139$. Q values are represented by slightly larger symbols.

Fig. 9. The true cold fission yields in percents for all fragmentations channels considered in Figs.7 and 8 computed with the LDM parameters, for spherical nuclei, with the inclusion of quadrupole deformations and with all deformations. In the bottom histogram, all yields $\leq 10^{-4}$ were set arbitrarily to $1.5 \cdot 10^{-4}$ to make easy the identification of the calculated fragmentation channels.

Fig. 10. The mass yields $Y_{A_1} = \sum_{Z_1} Y(A_1, Z_1)$ in percents, as a function of light fragment mass computed with LDM parameters. The same conclusions are obtained as before for separate charge and mass splittings. Calculations without deformations ($\beta_{2,3,4}=0$) enhance only the spherical region $A_1 \geq 106$; the inclusion of quadrupole deformations ($\beta_2 \neq 0$) enhances also the yields with $A_1 \geq 96$; for all deformations the main mass yields region becomes $96 \leq A_1 \leq 104$.

Fig. 11. The charge yields $Y_{Z_1} = \sum_{A_1} Y(A_1, Z_1)$, in percent, as function of light fragment mass computed with LDM-parameters. The same conclusions are obtained as before for separate charge and mass splittings. The calculations with no deformations ($\beta_i=0$) enhances only the yields with $Z_1 \geq 42$ and 44. The quadrupole deformations enhance also $Z_1=38$ and 40. The inclusion of all deformations enhances mainly the yields with $Z_1=38$ and 40.

Fig. 12. The geometrical parameters of the HF one-body densities, i.e. the reduced radii (r_n, r_p) and the diffusivities (a_n, a_p), for 162 light or heavy fragments included in the splittings represented in Figs.7 and 8. The parameters were obtained by fitting the HF one-body densities with Fermi density distributions in the range 2-18 fm. The effect of partial filling of nuclear subshells is clearly seen.

Fig. 13. The barrier heights computed with the HF parameters for Fermi one-body densities represented separately for odd Z and even Z . Successively we give the barrier heights for spherical fragments, for quadrupole, octupole and hexadecupole deformations together with the Q -values for the splittings considered in Figs.7 and 8. The lowest barriers are for $95 \leq A_1 \leq 103$ (Z -odd) or 104 (Z -even)

Fig. 14. The ternary yields in percents for the true cold ^{10}Be -ternary splittings computed with the HF parameters for different deformation sets : spherical ($\beta_i =$

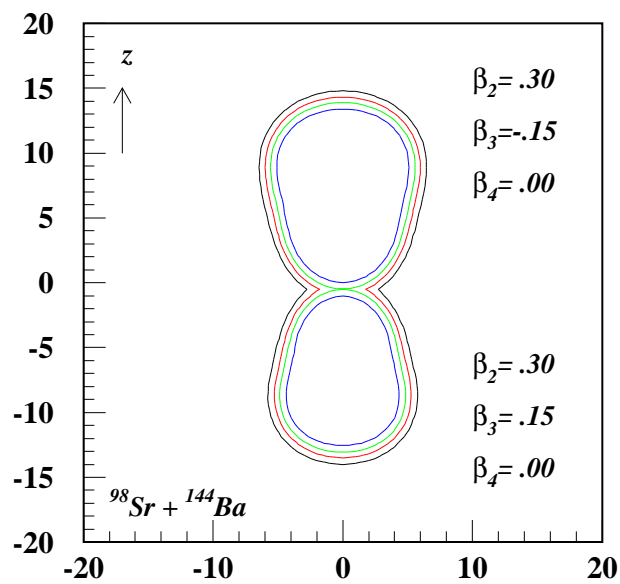
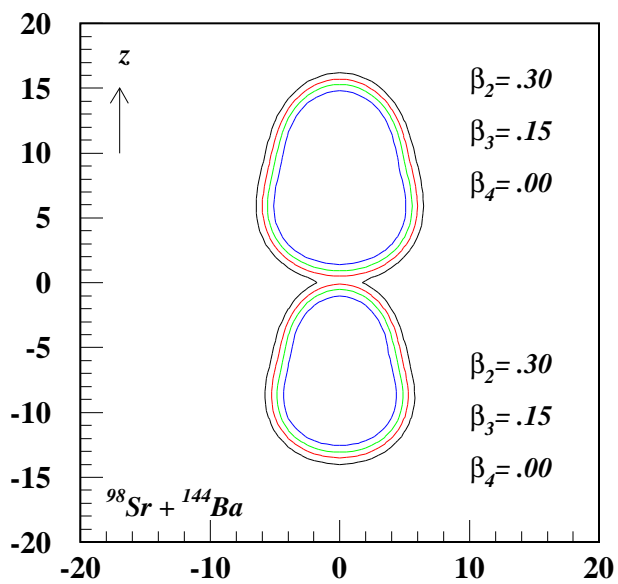
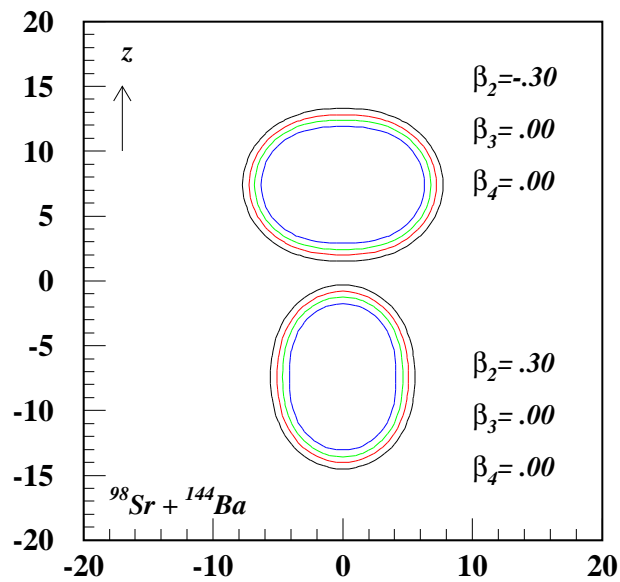
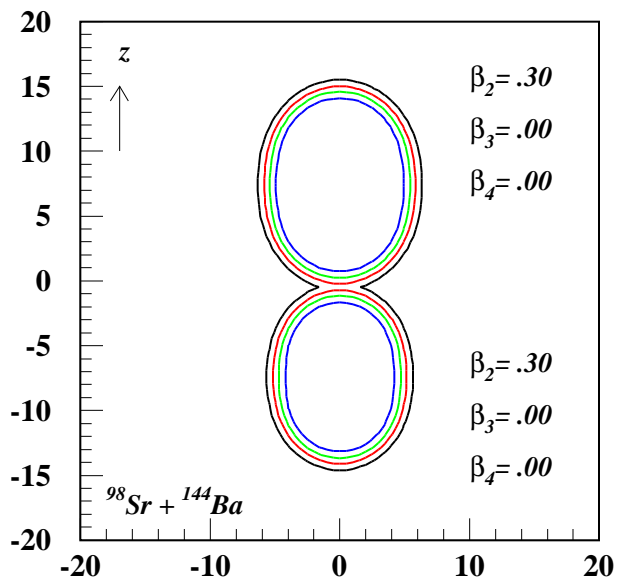
0), prolate ($\beta_2 \neq 0$) and all deformations ($\beta_2 + \beta_3 + \beta_4$). The results are similar with LDM-ternary yields represented in Fig.9. In the bottom histogram, all yields $\leq 10^{-4}$ were set arbitrarily to $1.5 \cdot 10^{-4}$ to make easy the identification of the calculated fragmentation channels.

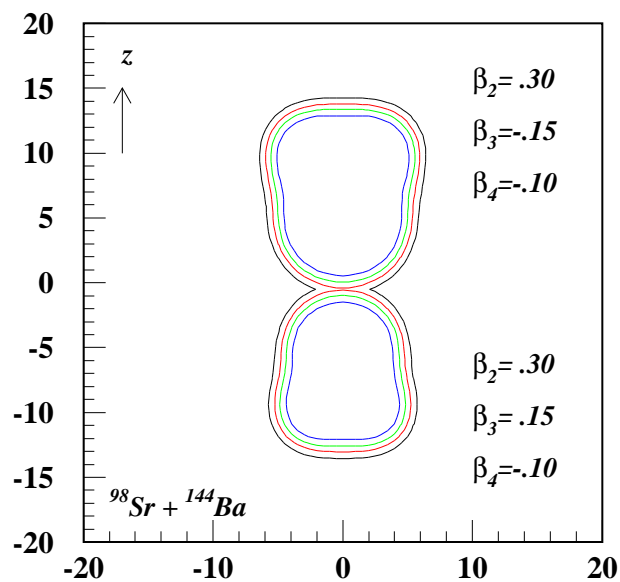
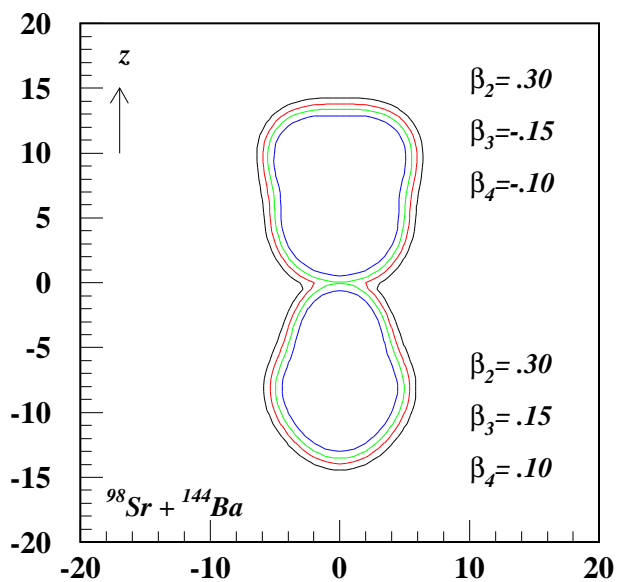
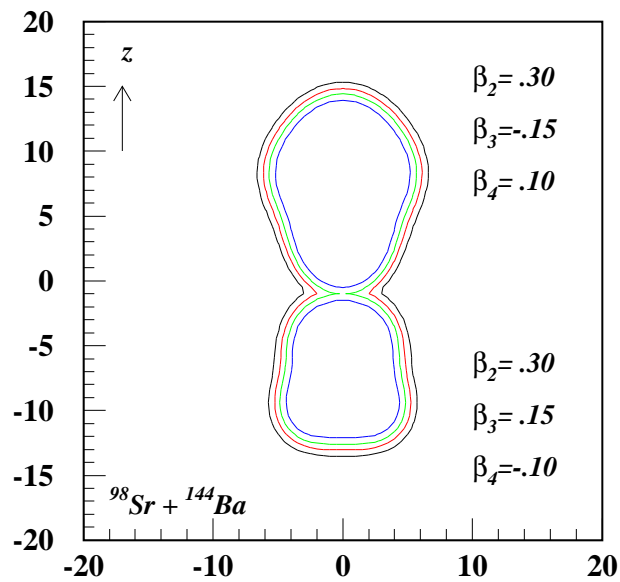
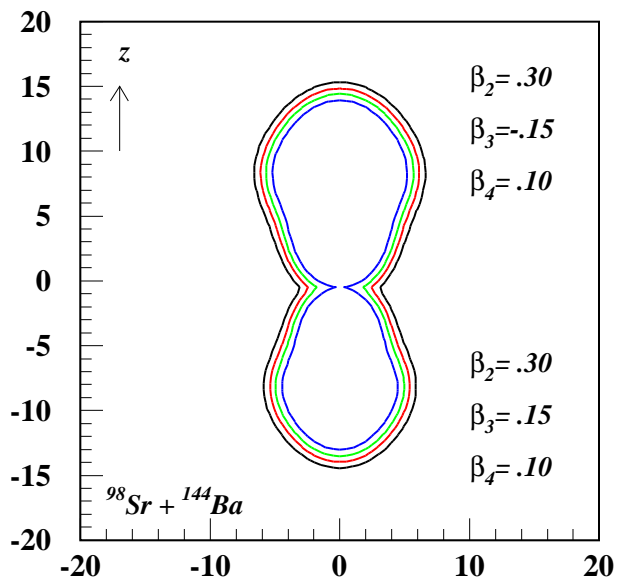
Fig. 15. The inner turning point (r_1), the outer turning point (r_2), the radius of the HF barrier heights (r_s) and the touching radius $r_t = (r_{A_1}^2)^{1/2} + (r_{A_2}^2)^{1/2}$ as function of light fragment mass. We denoted by open symbols odd Z fragments and by full symbols even Z fragments. The lines connect the symbols with the same Z . We can see that r_t is a smooth function of A_1 , that r_1 and r_b are strongly influenced by deformations and r_2 reflects the odd-even staggering of Q -values.

Fig. 16. The mass yields in percents $Y_{A_1} = \sum_{Z_1} Y(A_1, Z_1)$ computed with the HF one-body density parameters for different assumptions concerning the fragment deformations: spherical fragments ($\beta_i = 0$), quadrupole fragments ($\beta_2 \neq 2$), and all deformations ($\beta_2 + \beta_3 + \beta_4$). Similar with mass yields for LDM parameters we obtained for spherical fragments only for the spherical region $A_1 \geq 106$, for prolate fragments additional lighter yields for $A_1 \geq 96$ and for all deformations the mass yields are concentrated in the region $96 \leq A_1 \leq 104$

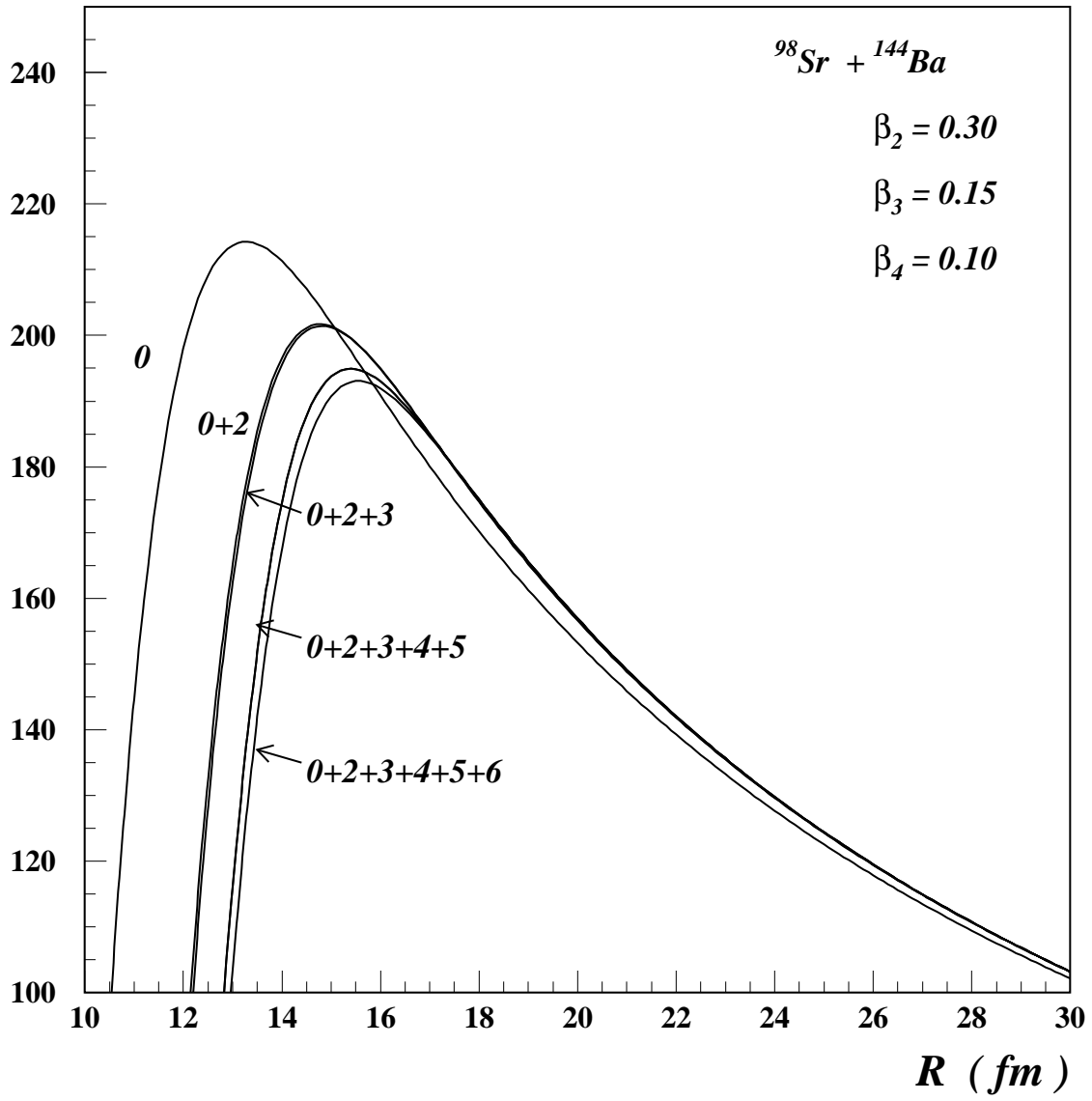
Fig. 17. The charge yields in percents $Y_{Z_1} = \sum_{A_1} Y(A_1, Z_1)$ computed with HF one-body density parameters as a function of the light fragment mass for different assumptions concerning the fragment deformations. For spherical fragments we have charge yields only for $Z_1=42$ and 44 . For prolate fragments the mass yields start with $Z_1=38$ and 40 . For all deformations the main charge yields are for $Z_1=38$ and 40 .

Fig. 18. The cold fission yields at excitation energies $E^*=1,3$ and 5 MeV, i.e. with modified penetrabilities due to the β -stretching and multiplied by level densities for all fragmentation channels in Figs.7 and 8. In the bottom histogram, all yields $\leq 10^{-13}$ were set arbitrarily to $1.5 \cdot 10^{-13}$ to make easy the identification of the calculated yields. We can see that fission yields are increasing with the excitation energy and that odd Z or/and odd N splittings are larger than the even ones.





M3Y - folding multipoles (MeV)



M3Y - folding multipoles (MeV)

